ABSTRACT

The subject of this theses is a growing of Yttria Stabilized Zirconia (YSZ) and its characteristics as an electronic material. The YSZ films were produced by a magnetron sputtering process and data were collected and examined. Characterization of the film consisted of x-ray diffraction, growth rate, current leakage, C-V characteristic, and relative permittivity. Some films were grown with a thickness under 40 Å and changes with thickness were recorded. It was observed that the ω peak characterization was changing with thickness in a range from about 130 to 170 Å. The ω peak below this range produced narrower FWHM values around 0.6 - 0.7˚ with steep peak sides. Above this range, a wide ω peak began to appear and continuously covered the narrow peak completely. While the characterization as a crystalline material was a success, its characterization as a gate material was simply unacceptable for some samples. The high amount of a trap charge shifted the flat band voltage more than a 1 V to -2 V, current leakage was up 0.35 A/cm^2 and its C-V characteristics showed an unnatural behavior. The measured relative permittivity for SiO_2 was about 10 times lower for the thickness 124 Å and 20 times lower for the thickness 53 Å. A few samples were found to exhibit the low leakage current value in the range from 10^{-5} to 10^{-5} A/cm^2.

TABLE OF CONTENTS

LIST OF TABLES

LIST OF FIGURES

INTRODUCTION

One of the main issues that have hindered the miniaturization of the MOS devices beyond the 0.1 μm range is the gate dielectric. Silicon dioxide has been the friendliest dielectric for the past 50 years but unfortunately it seems like we need to look for a material with higher dielectric constant than the silicon dioxide, since the leakage current rises to 1-10 A/cm^2 for SiO_2 gates below 20Å. Materials with higher dielectric constant have been suggested as alternative gate dielectrics, such as Ta_2O_5, TiO_2, Y_2O_3, ZrO_2, $ZrSi_xO_x$, etc. However, several of these materials are not thermally stable on silicon and SiO_2 is formed between the two material films during a deposition or annealing. The resulting gates have reduced effective capacitance and the amorphous SiO_2 layer leaves dangling bonds that may results in electronic defect states [1].

Yttria Stabilized Zirconia (YSZ) has reported relative permittivity of k = 25 - 29.7 and has both high thermodynamical stability in contact with silicon (even at 1000 ˚C) and has sufficiently large electron barriers for use as an alternative gates oxide [1]. Finally, the material can be grown epitaxially on monocrystalline Si, and it is not too expensive. That is why YSZ is very promising gate material for the under 0.1 μm CMOS technology.

YSZ has been used in the oxygen sensor industry or as a buffer layer for growth of superconductors on Si, but to date no CMOS integrated circuit (IC) have been produced with YSZ. Nevertheless, previous investigations have reported measurements of current leakage, C-V characteristic, and a relative permittivity.

One goal is to find a suitable technology to grow high quality epitaxial films of YSZ. Magnetron Sputtering is one possibility due to its simplicity, which is used widely across the field of IC manufacturing. There is the potential disadvantage however that the silicon surface may be damaged by deposition process.

I. PROPERTIES OF GATES

The key guidelines for selecting a gate dielectric are a) permittivity, band gap, and band alignment to silicon, b) thermodynamic stability, c) film morphology, d) interface quality, e) compatibility with the current or expected materials to be used in processing for CMOS devices, f) process compatibility, g) reliability [1, p. 5243].

The use of amorphous, thermally grown SiO_2 has advantages in the microprocessing as a thermodynamically and electrically stable when placed in contact with Si, and is known to produce excellent electrical properties. This means that is a big challenge for any alternative dielectric material to compete with existing SiO_2 technology.

The YSZ has higher relative permittivity, k = 25 – 27 for bulk and about 16 [2] for a thin film.

The result of the higher permittivity is that a film can be deposited to a greater thickness according to following

$$C/A = t_{eq}/k_{ox} = t_{high\text{-}k}/k_{high\text{-}k} \quad (1)$$

and after manipulation

$$t_{high\text{-}k} = k_{high\text{-}}k/k_{ox} * t_{eq} \qquad (2)$$

where $k_{ox} = 3.9$

The greater film thickness is an advantage because the reliability of the film increases with thickness.

Another crucial property is a current leakage. Ultrathin silicon oxide (13 – 15 Å) gets high leakage current densities of 1 – 10 A/cm^2 compared to required ~10^{-3} A/cm^2. The leakage current increases as thickness decreases [1, p. 5266] as a direct result of tunneling. The process of tunneling has been described with the following relationship [1]:

$$J_{DT} = A/t^2_{diel} * \exp[-2*t_{diel}*(2*m*q/\hbar^2*\{\Phi_B\text{-}V_{diel}/2\})^{0.5}] \quad (3)$$

where A = constant

t_{diel} = physical thickness of dielectric

V_{diel} = voltage drop across the dielectric

m = electron effective mass in the dielectric

This equation points to a higher thickness as a prevention of the gate current leakage. There is another physical phenomena related to the thickness, that is the effective electric field in the channel region. The higher electric field pulls the carriers in the channel closer against the dielectric interface, which causes increased phonon scattering and by this a decrease in the channel carrier mobility. At very high electric in the channel, interface roughness scattering further reduces carrier mobility. Since zirconium has four valence bands as does silicon, an epitaxial film would lower the interface scattering because of no free bonds in interface region. One must be careful however with conditions used in measurements, since the leakage current for the same material varies widely depending on surface preparation, deposition method, conditions, etc.

Another fact speaks in favor of YSZ is its relative permittivity. This constant is lower in a thin film (k = 16) than in a bulk (k = 25–27) and it has been reported [2] that the upper limit for a CMOS structure would be limited to k ~ 20 due to fringing field induced barrier lowering at the drain region. The constant must be balanced against the barrier height Ψ_B for the tunneling process, too. The barrier height for electrons traveling from the Si substrate to the gate is given by $\Delta E_C = q^*[X-(\phi_M-\Psi_B)]$ and for the opposite direction it is Ψ_B (Fig. 1). If the experimental ΔE_C value for a dielectric is less than 1.0 eV, it will be excluded from a gate application because of either thermal emission or tunneling lead to a high leakage current. The ΔE_C for YSZ is about 1.5 eV (Fig. 2, [1]).

A gate material must be thermodynamically stable on Si. Most materials with a high dielectric constant are unstable on Si creating SiO_2 at the interface or decomposing to SiO_2 and metal oxide. YSZ is essentially transparent to oxygen ions, which may lead to an interface layer of SiO_2. A lack of excess oxygen used in the deposition process

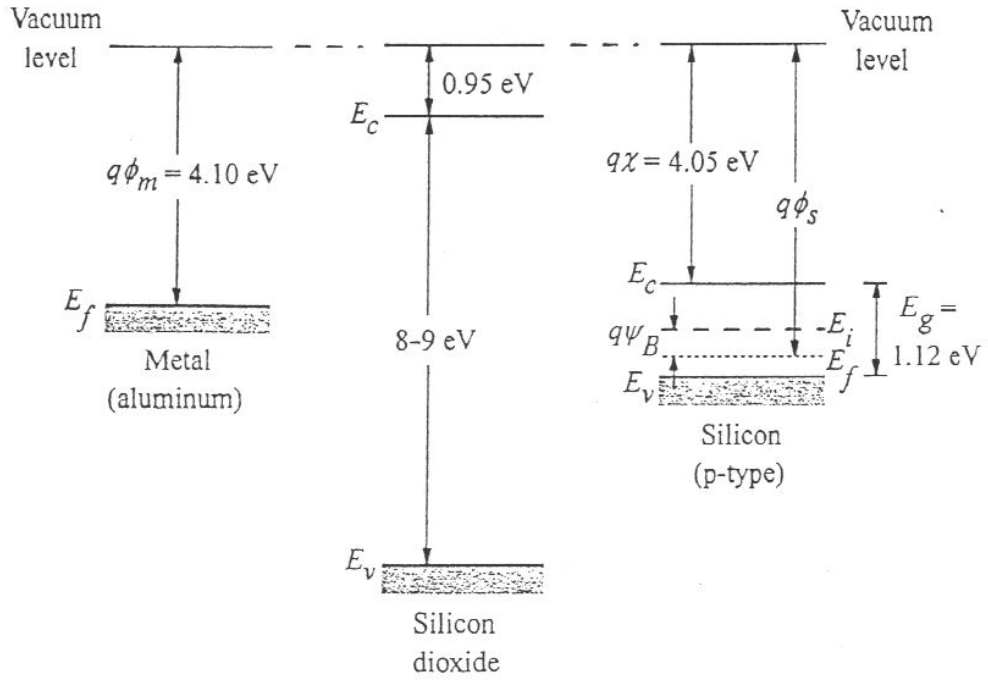

Fig. 1

Energy-band diagrams for p-type semiconductor substrates

may prevent its formation. On the other hand, a lack of the oxygen itself will support Zr-Si bond. A careful procedure is required to produce a film with the desired parameters.

Other two crucial factors, a process compatibility and reliability, are beyond the scope of this investigation.

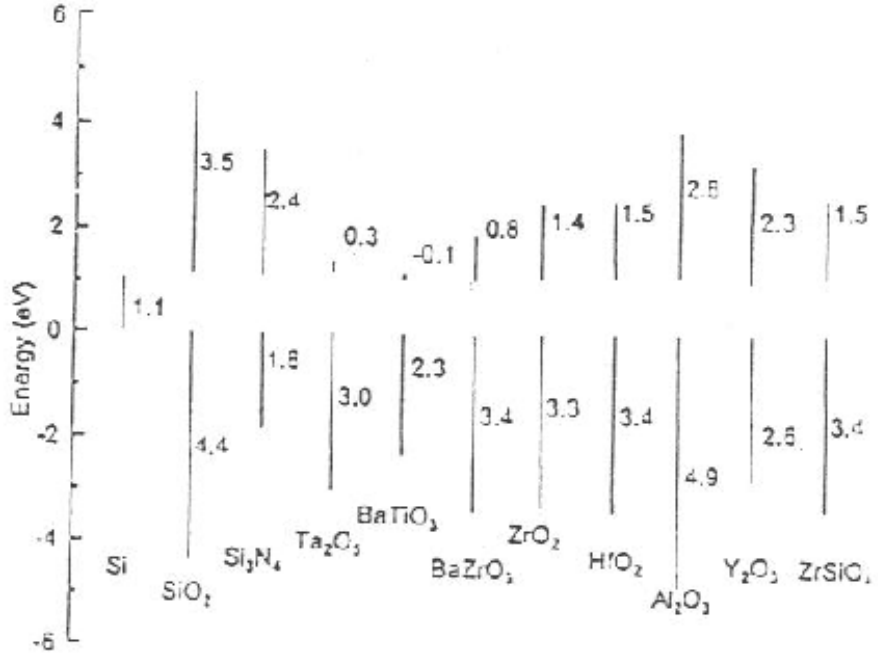

Fig. 2

Barrier height for different gate materials

II. YTTRIA STABILIZED ZIRCONIA (YSZ)

Zirconia (ZrO_2) is transparent material known as the artificial diamond. When an amount of yttria (Y_2O_3) is $7\%_{mol}$ or more, then zirconia changes its crystal structure from monoclinic ($a_0 = 5.1454$Å, $b_0 = 5.2075$Å, $c_0 = 5.3107$Å, $\beta = 99^\circ 14'$, Fig. 3 [3]) to simple cubic (lattice parameter $a = 5.122 + 2.651*10^{-3}*X$ [Å], where $X = \%_{mole}$ of yttria) and this material is called YSZ. It is a stiff material with elastic constants $c_{11} \approx 400$, $c_{12} \approx 100$, and $c_{44} \approx 60$ [GPa] [4]. Its conduction band offset, $\Delta E_C \approx 1.5$ eV [1, p. 5267] is high enough and its relative permittivity is approximately 20. Another advantage of YSZ is that Zirconium has four valence bands as does Si. This means that if a film is grown epitaxial on Si, then there is potential for no dangling bonds. This both lowers the penetration of mobile charge from an inversion layer into the gate and increases speed of the charge due to a lower probability of scattering. Another plus of the material is that it is stable on silicon even at temperature as high as 1000 ˚C.

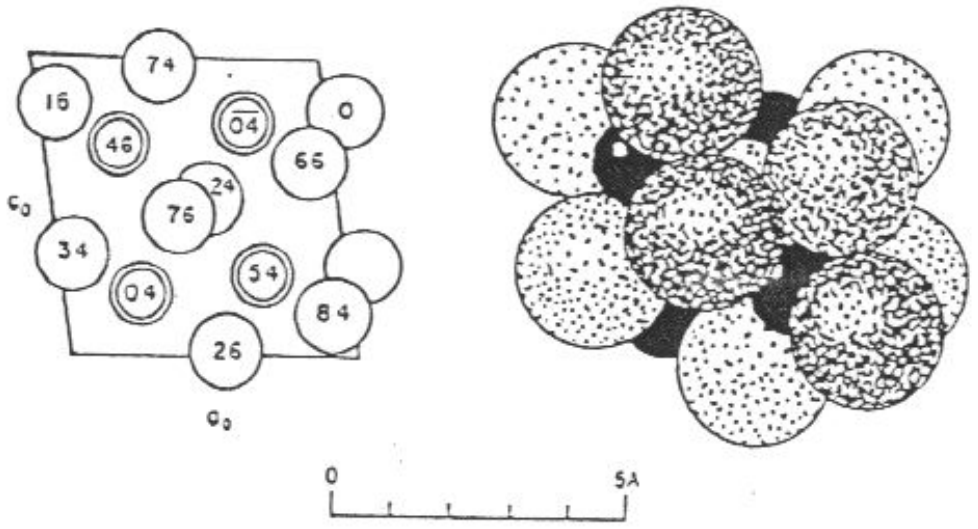

Fig. 3

Left – The ZrO_2 arrangement projected along the b_0 axis. The zirconium atoms are doubly ringed. Right – A packing drawing of the arrangement viewed along the b_0 axis. The small black circles are zirconium.

III. EXPERIMENTAL PROCEDURE

A. Deposition Chamber

The sputter deposition chamber used to deposit the YSZ material films is shown in Fig. 4. The figure shows a vertical cut of the magnetron sputter system. The target's front side is aimed towards a Si sample as much as possible to make material sputtered from the YSZ target travel to the sample with as little loss as possible. The target is made by sintering ZrO_2 and Y_2O_3. The content of Y_2O_3 is $8\%_{mole}$.

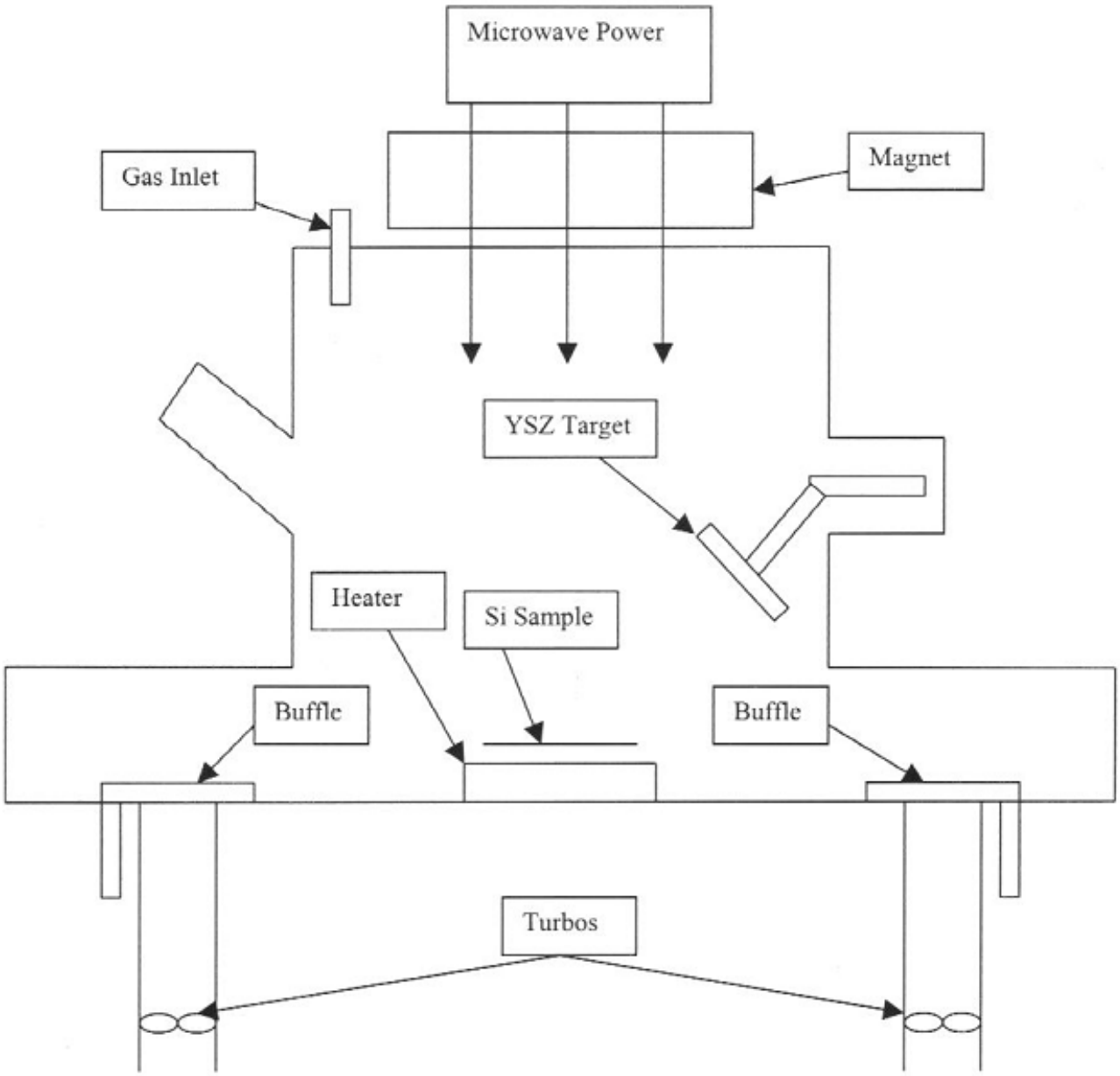
Microwave Power
Magnet
Gas Inlet
YSZ Target
Heater
Si Sample
Buffle
Buffle
Turbos

Fig. 4

The Schematic Cut of Magnetron Sputter Reactor

The reactor pressure measured at the start of this investigation was found to be in the 10^{-6} torr range. Some time into the investigation a leak appeared and the pressure changed to the 1.2 – 1.9 on 10^{-5} torr scale. It did not appear to influence the quality of deposited films.

The Ar gas was brought in via an inlet at the top where the magnet was located. At the bottom there are two outlets. Both can be continuously covered with baffles to adjust pressure to a desired level. The pressure can also be changed by flow rate of gases into the chamber. Under each baffle there is a turbo, which is in theory capable to keep the pressure at the 10^{-7} torr scale.

A heater is located in the middle near the base of the chamber. The heater is a ceramic plate with carbon leads through its body. It can be heated only in an oxygen free environment, otherwise the leads will burn up. The heater sits in an assembly, where a sample is held on a boat. The sample itself is 28 mm wide and 42 mm long. For some experiments the sample was cut to two halves, one part was etched in HF, the other not, and both were then put on the boat. The two different samples were used to consider the effect of a native oxide on film growth.

B. Film Growth Conditions

The YSZ films were deposited at pressure about 13 mtorr in present of Ar plasma. A magnet current was turned to 159 A and the RF sputter gun was driven at a power of 300 W with a reflective power less than 10 W. The reflected power was minimized with a matching network. The principle is to match real and imaginary circuit parts of both the box and the target. Temperature was adjusted to a desired value with a rheostat and was kept steady during a deposition step. Its range was from a room temperature (the heater off) to 800 ^{o}C. A deposition time was counted from the instant when the magnet current was set to 159 A and stopped with switching the RF gun off. The time was short as 60 s and as long as 180 s for samples grown to study the growth rate and crystallography. Films, which were grown for a longer time, were grown in a deficit oxygen mode, up to 4 min. (240 s). Some films were deposited both in the deficit oxygen mode and in an oxygen/argon environment with a total time from 2 min. to 4 min. The modifications in procedure were used to find the best way to grow thin films but no significant

differences were observed. The films with longer deposition time were grown 4 min. in the oxygen deficit mode and then with the O_2 / Ar line on, as seen from the procedure. The total time did not exceeded 24 min.

Procedure:

1 A sample was either etched in HF to get rid of native oxide or not to leaving a native oxide in place.

2 The sample was put into the sputtering chamber and heated to desired temperature. A waiting time of 20 min. was used.

3 After 20 min., an Ar-line mass flow controller was switched on, and by using both baffles the pressure was adjusted to about 5 mtorr.

4 Pressure was increased to 13 mtorr by increasing the flow rate of Ar (from 20 sccm to about 40 sccm).

5 A magnet current was turned to 159 A.

6 The RF gun was switched on.

7 After a measured deposition time, the RF gun was switched off, a magnet current was adjusted to a zero, the Ar flow rate was decreased to 20 sccm, the Ar gas line was turned off, and the heater was turned off as well.

8 The sample was removed from a reactor chamber.

For the thicker films requiring a longer deposition time the above procedure was modified as following:

7 After 4 min., the ECR was switched on, the right baffle was adjusted to decrease the pressure, the Ar / O_2 line was turned on, the flow rate of Ar was decreased to 20 sccm, and the right baffle was adjusted to establish a pressure of 5 mtorr in the reactor chamber.

8 After a measured time, up to 20 min., everything was switched off and the sample removed.

C. Structural Analysis

A general relation, which will predict a diffraction angle for any set of planes is obtained by combining the Bragg law, $\lambda = 2*d*\sin\theta$, and the plane-spacing equation. For a cubic crystal the plane-space equation is

$$1/d^2 = (h^2 + k^2 + l^2)/a^2 \quad (4)$$

and by combining them

$$\sin^2\theta = \lambda^2/4* (h^2 + k^2 + l^2)/a^2 \quad (5)$$

This equation predicts, for a particular incident wavelength λ and a particular cubic crystal of unit cell size *a*, all possible Bragg angles at which diffraction can occur from the planes *(hkl)* [5, p. 91]. The 2θ-ω and ω scans were performed on Philips X-ray machine to determine the epitaxial quality of the deposited YSZ material film. The measured lattice constant could be used to calculate the mole concentration of the yttria in the YSZ film lattice parameter, and from the lattice parameter, mole concentration of yttria in YSZ film. The thickness of the film was measured with an ellipsometer. The thinnest film successfully measured was 39 Å, while thinner films resulted with as a bad calculation results.

D. Electrical Properties

The capacitance-voltage (C-V) technique relies on the fact that the width of a reverse-biased space-charge region (scr) of a semiconductor junction device depends on the applied voltage. This scr width dependence on voltage lies at the heart of the C-V technique [6, p. 63]. Many C-V measurements are made with no corrections or with estimated errors. One of the potential errors in using this technique is a series resistance. If the back contact resistance r_C is a problem (Fig. 5a), it may be advantageous to leave the oxide on the back surface and place the wafer on a probe station, thus making a large-area capacitive back contact (Fig. 5b). The contact capacitance C_c in much

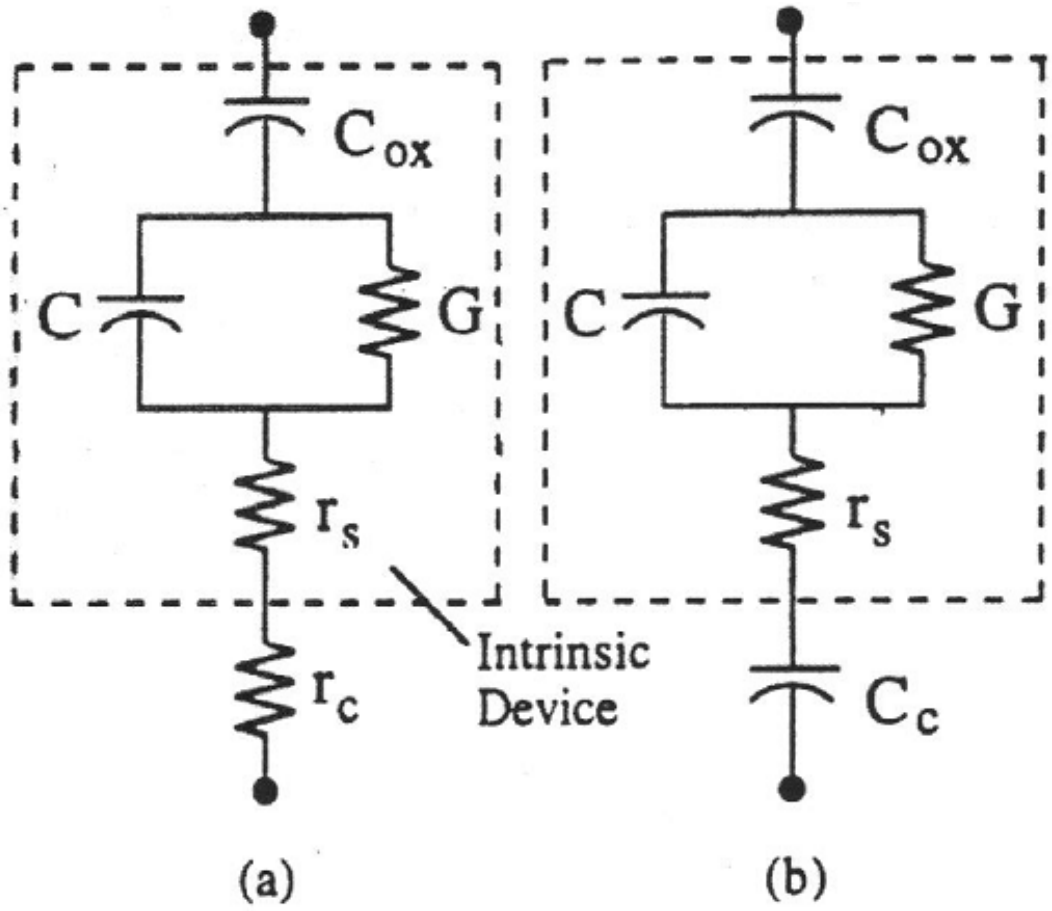

Fig. 5

Schematic Circuit Setup of Measurements

larger than the device capacitance because its area is usually the area of the entire sample. Such a large capacitance approximates a short circuit. A *p-n* or Schottky diode consists of a junction capacitance C, a junction conductance G, and a series resistance r_s as represented in the Fig. 6a. Capacitance meters assume the device to be represented by either the parallel equivalent circuit (Fig. 6b) or the series equivalent circuit (Fig. 6c). Combining these two circuits into one results in the mathematical description below, which permit C_p, G_p, C_s, and R_s to be written as

$$C_p = C/[(1 + r_s*G)^2 + (0\omega*r_s*C)^2] \quad (6)$$

$$G_p = [G*(1 + r_s*G) + r_s*(\omega*C)^2]/[(1 + r_s*g)^2 + (\omega*r_s*C)^2] \quad (7)$$

$$C_s = C[1 + G/(\omega*C)^2] \quad (8)$$

$$R_s = r_s + 1/G/[1 + (\omega*C/G)^2] \quad (9)$$

Both measured capacitances C_p and C_s deviate from C at high G.

The method of ratios was used to compute the dielectric capacitance. It is supposed that the gate capacitance C and the gate conductance G are constant for the entire range of frequencies. Then two set of data are substituted to the Eqn. 10 and the two compared:

$$\omega*C/G = F/[1-G_m*r_s*(1+F^2)] \quad (10)$$

where $F = \omega*G_m/C_m$.

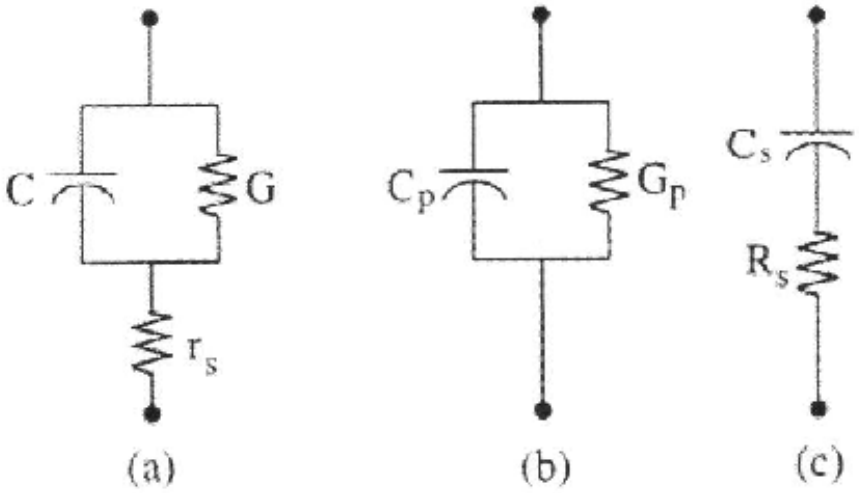

Fig. 6

Equivalent Circuits for C-V Measurements

The $(\omega_2*C/G) / (\omega_1*C/G)$ is a ratio of the two frequencies that is LHS of the equation and the numbers (ω_1*C_{m1}/G_{m1}) and (ω_2*C_{m2}/G_{m2}) are substituted to its RHS. The only unknown is the series resistance r_s. After solving for the r_s, the capacitance was computed by Eqn. 6.

Another procedure to obtain the dielectric capacitance is to plot capacitance versus voltage (C-V curve). The bias voltage is swept from $-V_g$ to $+V_g$ with a superimposed small amplitude ac voltage of typically 10-15 mV amplitude. The ac voltage is necessary to measure the capacitance, while the dc voltage determines the bias condition. If the dc voltage is swept sufficiently slowly to allow the inversion charge to form and if the ac voltage is of a sufficiently low frequency for the inversion charge to be able to respond to the ac probe frequency, then the low-frequency curve is obtained. If the dc voltage is swept sufficiently slowly to allow the inversion charge to form but the ac probe frequency is too high for the inversion charge to be able to respond, then the high-frequency curve is obtained. The deep-depletion curve is obtained for either high or low frequency when the dc sweep rate is too high to permit the formation of an inversion charge (6, p. 344). A typical C-V curve of a p-type MOS capacitor is shown in Fig. 7.

The empirical relation of the Eqn. 11 was use to verify reliability of the C-V curves.

$$\log[N] = 30.38759 + 1.6828*\log[C_1] - 0.037177*(\log[C_1])^2 \quad (11)$$

Measurements to determine a relative permittivity k_{YSZ} and a gate current leakage were run on the HP-4275 Multi-Frequency LCR Equipment. The relative permittivity k_{YSZ} was computed from Capacitance vs. Frequency Plot with frequency of 1 MHZ.

The gate current leakage was measured on the same equipment and a I_{gate} vs. V plot was generated.

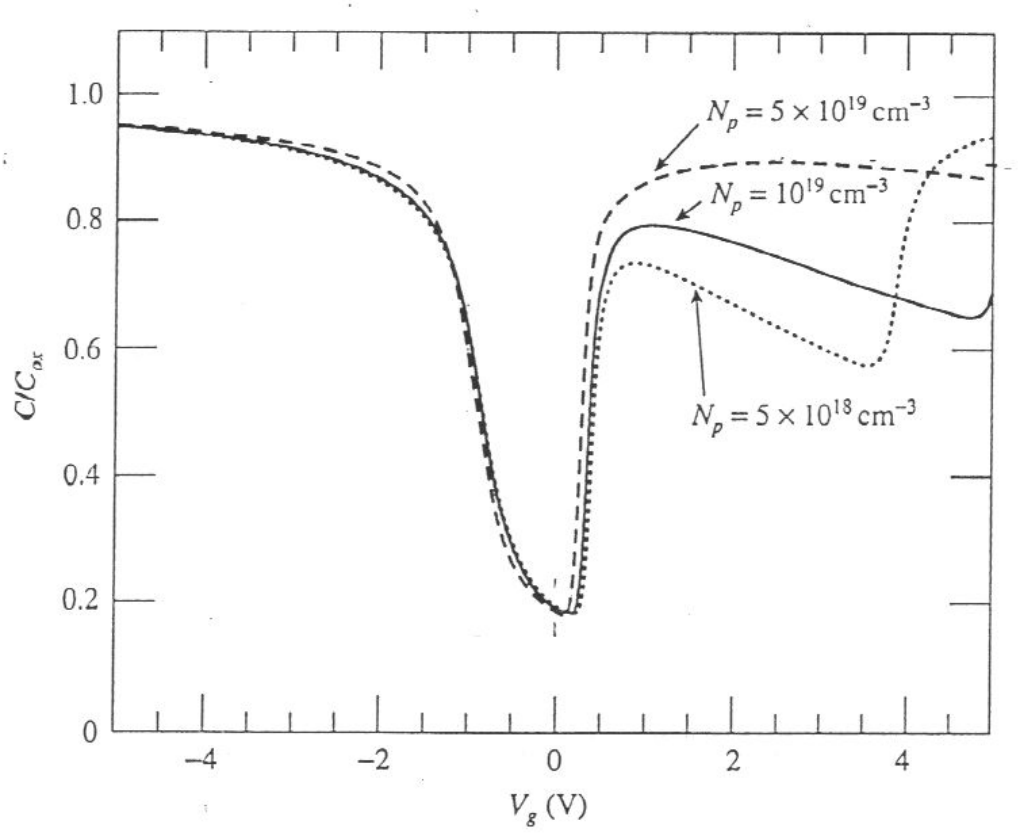

Fig. 7

The C-V Curve of p-type MOS for different dopings

E. Growth Rate

In chemical reactions considered, generally,

$$\text{A} + \text{reactants} \leftrightarrow \text{products} \quad (12)$$

any species can be taken to compute a reaction rate constant *k,* which is a function of the

concentrations (activities) of various species involved in the reaction, i.e. the disappearing species A,

$$-r_A = [k(T)][fn(C_A, C_B, \ldots] \quad (13)$$

The algebraic equation that relates $-r_A$ to the species concentrations is called the kinetic expression or rate law [7, p. 62].

The reaction rate constant *k* is not a real constant, it's independent to concentrations of species involved in reaction and strongly depends on temperature. As well as it depends on a catalyst, total pressure, ionic strength, and environment, but with much smaller effect that it can be assumed the reaction rate constant depends only on temperature. The temperature dependence can be written as,

$$k(T) = A*e^{-E/R/T} \quad (14)$$

where A = preexponential factor

E = activation energy [J/mole]

R = the gas constant = 8.314 J/mole/K

T = absolute temperature [K]

The dependence of the reaction rate $-r_A$ on concentrations of the species present, $fn(C_j)$, is almost without exception determined by experimental observation [7, p. 66]. The most general form is the product of concentrations of individual reacting species, each of which is raised to a power, e.g.,

$$-r_A = k*C_A^{\alpha}*C_B^{\beta} \quad (15)$$

The exponents of the concentrations determine a reaction order. The order of a reaction refers to the powers to which the concentrations are raised in the kinetic rate law [7, p. 66]. In the equation above, the reaction is α order with respect to reactant A, and β order with respect to reactant B.

The overall order of the reaction, *n,* is

$$n = \alpha + \beta \quad (16)$$

The units of the specific reaction rate, *k,* vary with the order of the reaction:

Zero-order:	$-r_A = k$	$k=[mole/(dm^3*s)]$	(17)
First-order:	$-r_A = kC_A$	$k=[s^{-1}]$	(18)
Second-order:	$-r_A = kC_A^2$	$k=[dm^3/(mole*s)]$	(19)
Third-order:	$-r_A = kC_A^3$	$k=[(dm^3/mole)^2*s^{-1}]$	(20)

where dm^3 means a cubic decimeter (1 dm^3 = 1 l).

For heterogeneous reaction, e.g. the Chemical Vapor Deposition (CVD), the growth rate is expressed as a deposition rate r_{Dep} [length/time]. A conversion to a molar rate ® = [mole/m^2/s]) is realized by multiplying by the molar density of deposited film.

The differential method was modified to compute the growth rate and activation energy. The modification was simply an exchange a length for concentration.

When a reaction is irreversible, then it is possible to determine the reaction order α and the specific rate constant by numerically differentiating concentration versus time, in our case, differentiating deposition length versus time. This is called the differential method of rate analysis. The method is applicable when reaction conditions are such that the rate is essentially a function of the concentration of only one reactant:

$$A \rightarrow \text{products} \quad (21)$$

Since the plasma deposition has only one product, YSZ, the method is applied to the only product. The number of reactant is unknown but their concentration during deposition is considered

constant.

Under these circumstances:

$$\text{reactants} \rightarrow \text{YSZ} \quad (22)$$

$$r_Y = k*d \quad (23)$$

where Y stands for YSZ and d = thickness of deposited film [Å]

For a constant-volume reactor, the growth rate equals the derivative of thickness with a respect to the time [7, p. 32]

$$r_Y = dC_Y/dt = dd/dt \quad (24)$$

and after substituting to (23)

$$dd/dt = k*d \quad (25)$$

After taking a logarithm of both sides

$$\ln(dd/dt) = \ln(k) + \alpha * \ln(d) \quad (26)$$

where a slope of plot is a reaction order α (Fig. 8).

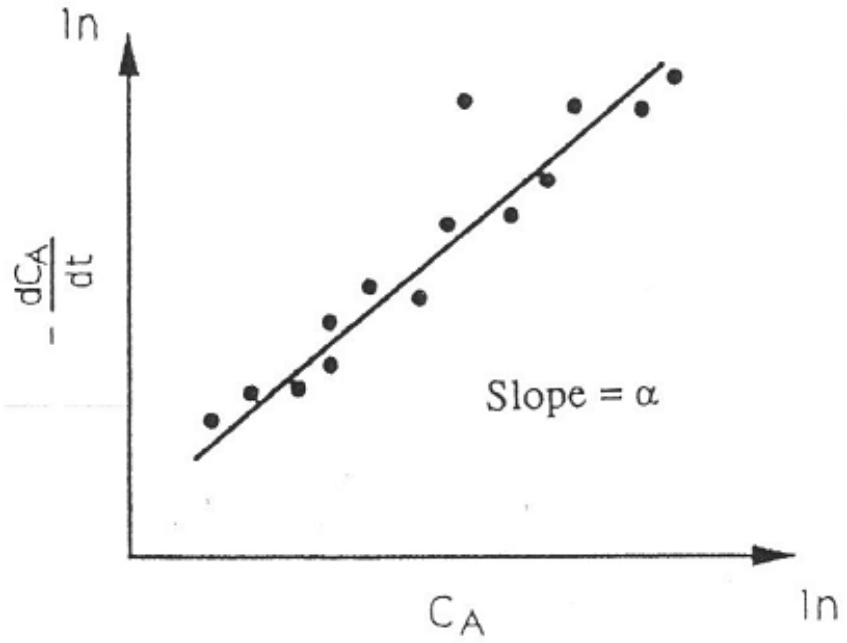

Fig. 8

The differential method to determine the reaction order

The quality of the deposited film is dependent on the growth rate of the film. When the deposition rate is slow enough, the atoms of the film receive enough time to arrange themselves on the surface and grow epitaxially on a highly oriented surface. If the growth rate is too high and the atoms do not have a time to set themselves in a highly oriented arrangement, then the film becomes polycrystalline. The overall mechanism is temperature dependent. A general function of quality vs. Temperature is showed in Fig. 9.

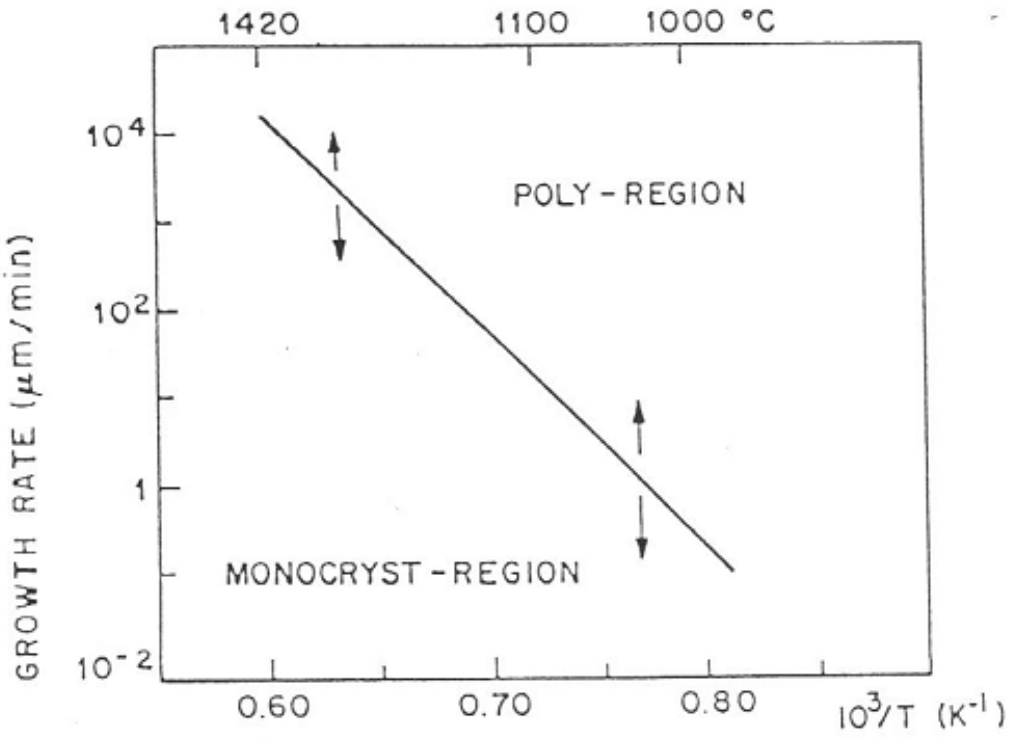

Fig. 9

The quality of film in dependence on the growth rate and temperature

IV. CHANGE OF 2θ-ω PEAKS WITH TIME

During the Spring semester the YSZ sputter target was moved from its original position to a position in which the growth rate decreased significantly. The advantage of this accident was that the quality of film improved with the FWHM of ω peaks hovering around 0.3˚, and intensities around 20,000 counts for film thickness just over 200 Å. The results were never repeated and they are summarized at the Table 1. What was observed at that time was that after about four weeks the x-ray peaks of some samples changed. The Si-prohibited peak that was originally of high intensity,

decreased in intensity and the YSZ peak that was originally low intensity became higher. The peak location was also observed to move with time. The "forbidden" Si peak moved from the <002> direction to the <111> direction and the YSZ peak, which originally showed about 30 $\%_{mole}$ of yttria lowered its yttria content. Unfortunately this was observed only with two samples (e.g. j007, see the Fig. 10). One sample showed no peaks after growing but both peaks were found after four weeks.

The change observed in these few samples suggested that the films grown under these conditions were metastable, which is seen from a calculation of lattice parameter and the $\%_{mole}$ of yttria in the zirconia as well from the fact that thickness increased by 6-10 Å. This is important because of consideration of evaluated temperature treatments, e.g. annealing, where this change would be accelerated and conditions would be changed dramatically, e.g. a lattice parameter.

V. CHANGE OF ω PEAKS WITH THICKNESS

After turning the YSZ target towards the location of the sample, the deposition time was decreased to get thinner films. When the deposited thickness was decreased to about 200 Å, the shape of the ω peak changed. With decreasing thickness another peak, more exactly, a peak with a different shape began to immerge. The new peak was much more narrow with FWHM in the range from 0.6 to 0.7˚. This is certainly an improvement over films with a thickness over 200 Å but still inferior to films grown in the Spring period. The results are collected in the Table 2, the Fig. 11 and 12. As observed from the set of plots and data, the FWHM improved dramatically for thickness under 100 Å, since the YSZ "copies" the substrate and accepts the lattice parameter of the <100> Si wafer. The YSZ grows with the Si lattice parameter up to about 100 Å and then the YSZ abruptly gains its bulk parameter without any continuous change as it was reported by Bardal et al [8]. The difference between this thesis and the study by Bardal et al is probably in the amount of oxygen involved in the procedures. Bardal et al reported a SiO_2 layer between the Si substrate and the YSZ layer. The YSZ could relax to its natural lattice parameter much early (5 - 7 nm) due to the SiO_2 layer. This phenomenon depends on the growth rate of the material film and the partial

Sample	date	d [Å]	2θ	ω	FWHM	T [˚C]	note
jiri004	4/13	206	32.93	17.74	0.28	852	no HF
jiri004	5/15	210	34.95				
jiri007	4/12	948	32.7	18.25	0.507	791	no HF
jiri007	5/12	985	34.77				
jk0416a	4/16	203	NA			791	
jk0416a	5/15	211	33.02	16.61	0.286		no HF
jk0416b	4/16	212	NA			791	
jk0416b	5/14	222	35.09	16.61	0.285		no HF
jk0418a	4/18	203	NA			728	
jk0418a	5/12	208	32.86	16.48	0.323		
jk0418b	4/18	213	NA	16.5		728	
jk0418b	5/12	219	32.93	16.47	0.281		
jk0419a	4/19	219	NA	16.61	0.305	728	
jk0419a	5/15	227	33.27	16.6	0.296		
jk0426a	4/26		NA			852	
jk0426a	5/12	930	32.91	16.42	0.277		

Table 1

Data of samples deposited in the Spring period

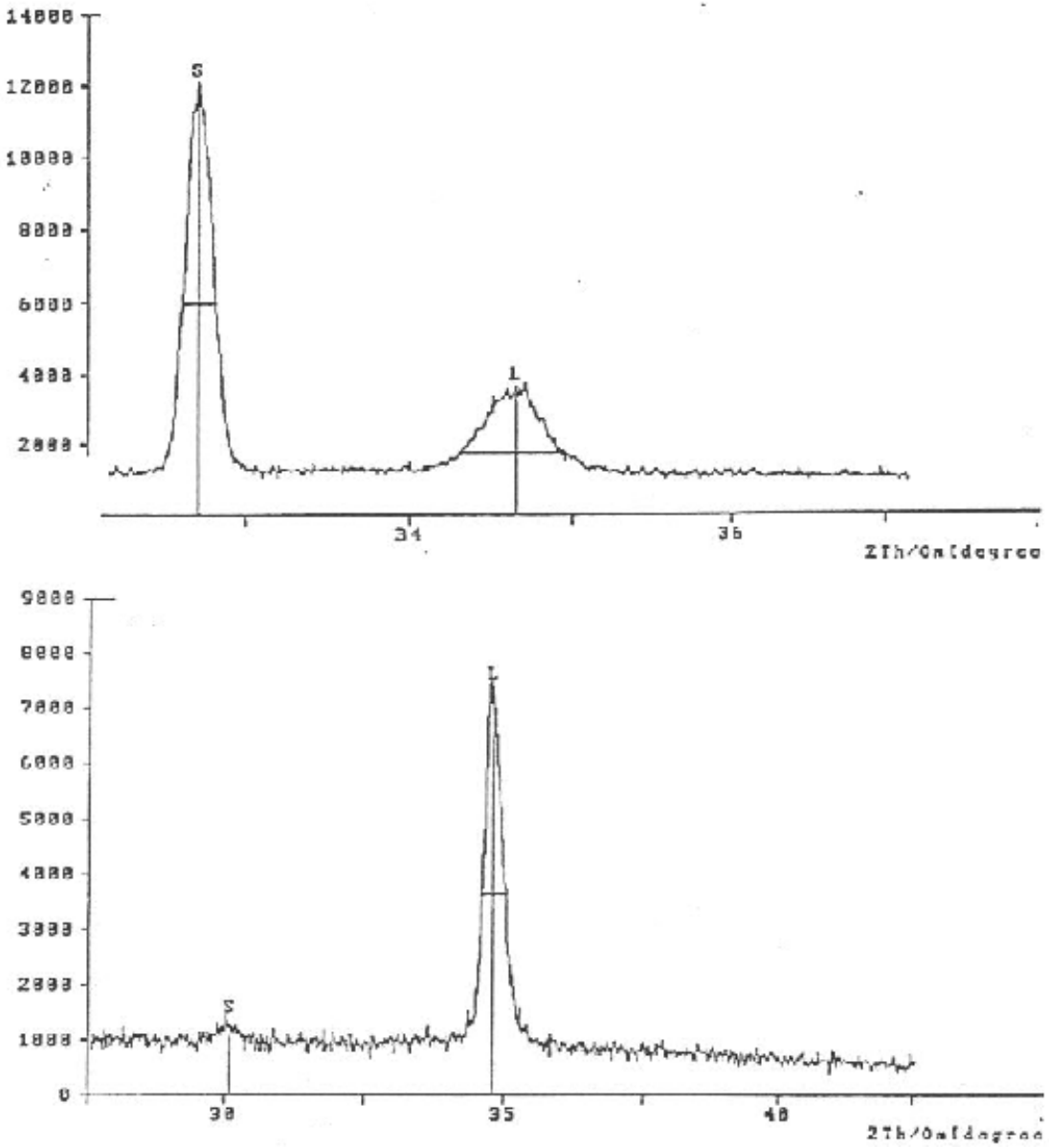

Fig. 10

The peak changes of the sample j007

Growing temperature = 850 ℃, thickness = 948 Å, just after deposition, 982 Å after four weeks

sample	T [°C]	thick [Å]	FWHM	Si-2θ-ω	YSZ-2θ-ω	a_{Si} [Å]	$a_{YS}Z$ [Å]	$\%_{mole}$ YSZ
jk10001a	666	62.4	0.64	32.98	NA	5.43	NA	NA
jk1002b	540	52.1	0.75	33.25	NA	5.39	NA	NA
jk0916c	800	122.0	2.99	33.02	34.97	5.42	5.13	2.3
jk0916e	800	111.0	3.20	33.07	35.03	5.41	5.12	0
jk0916d	800	172.0	2.53	32.90	34.88	5.44	5.14	7.0
jk0920a	800	119.0	3.09	33.07	35.02	5.41	5.12	0
jk0915b	800	407.0	1.78	NA	34.88	NA	5.14	7.0
jk0915f	800	375.0	2.18	33.07	34.89	5.41	5.14	6.5

Table 2

The sample data of different thicknesses

pressure of oxygen in the chamber. The samples from the Spring period has the Si lattice parameter for the thickness 200 Å and with the deposition procedure involving 20 min. Of the Ar/O_2 line on.

No experiment was conducted for the Spring samples to determine whether the SiO_2 layer was involved on not. The cause, which triggers the transition that widens the ω peak is probably a number of dislocations that appear when the growth rate continues.

VI. DETERMINATION OF GROWTH RATE

The deposition time was varied from 1 min. to 3 min. in 15 s and 30 s intervals. The thickness for 1 min. deposition was usually not available, probably due to a quality of deposited film. First, a linear fit was applied to thickness vs. time plots. The fitting number R was higher than 0.98 for all

sets of data but two and both runs were for samples with an HF dip and sample wafer was as a unit, it means the sample was not cut in half. Runs with samples cut in a half, where one half was etched in HF showed similar growth rates. The samples, which were not cut and a native oxide was left produced well behave trends but the initial layer of oxide was rather scattered and always higher than for cut pieces. The data does not yield either an exact thickness of the native oxide or the initial speed of deposition but shows that the thickness of the native oxide was in a range from 20 Å to 30 Å. It was observed that for etched samples the initial deposition occurred at a higher rate than that of the remaining deposition.

etched in HF showed similar growth rates. The samples, which were not cut and a native oxide was left produced well behave trends but the initial layer of oxide was rather scattered and always higher than for cut pieces. The data does not yield either an exact thickness of the native oxide or the initial speed of deposition but shows that the thickness of the native oxide was in a range from 20 Å to 30 Å. It was observed that for etched samples the initial deposition occurred at a higher rate than that of the remaining deposition.

A plot thickness vs. time was made for each run in hopes of determining the order of the reaction. A polynomial and linear fit were applied to the data. A starting point for the polynomial fit was added, namely thickness d = 0 at time = 0 for etched samples and initial thickness d_0 at time = 0 for native oxide samples. From the polynomial best fit curve, a derivation was taken and a plot $d\mathrm{d}/d\mathrm{t}$ vs. thickness was made. The slope of the plot should give the order of the chemical reaction. As seen from the plots, it was not possible to determine a slope mainly because of physical aspects such as the magnetic field and power of the sputtering gun made much stronger influence on the rate than the chemical activities of chemical compounds (Fig. 12). This is even true for samples that were not etched and where the chemical reaction

$$2SiO_2(s) + Zr(g) \rightarrow 2SiO(g) + ZrO_2(s) \quad (27)$$

occurs.

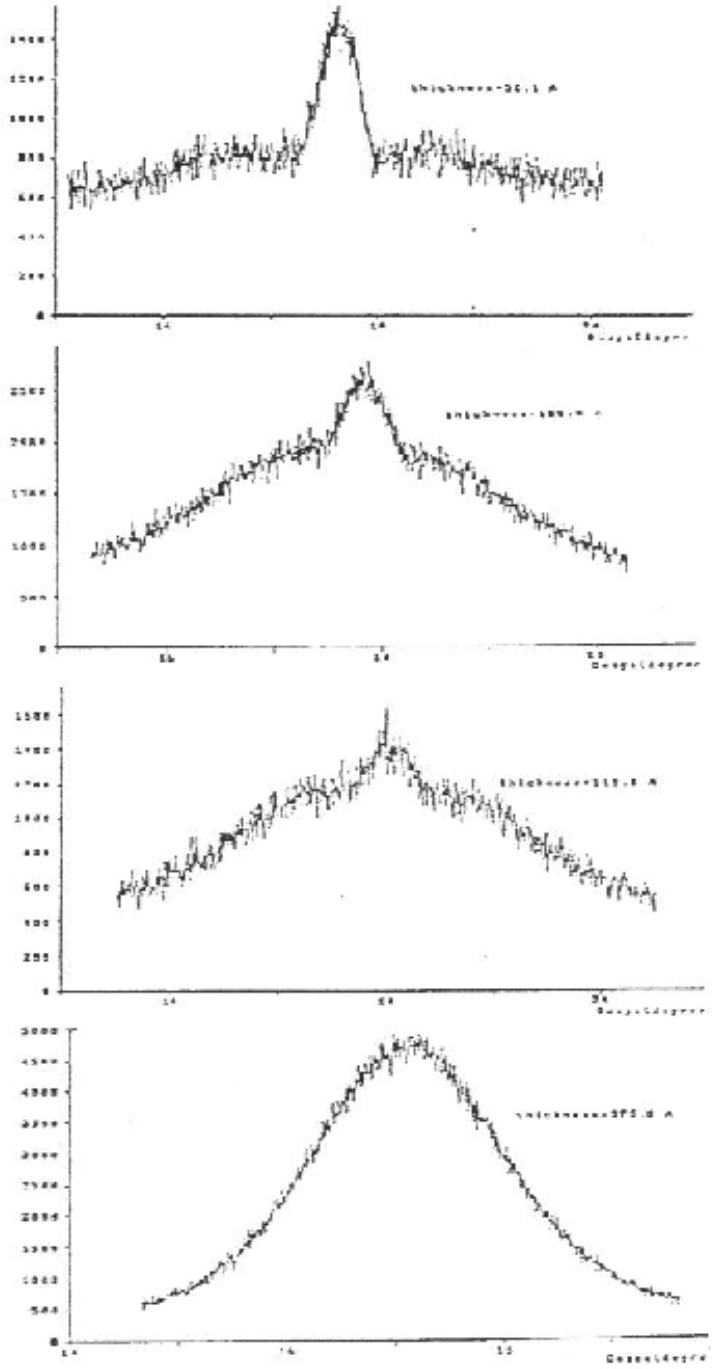

Fig. 11

The ω peaks for thicknesses (from above) [Å]: 62.4, 111.0, 119.0, 375.0

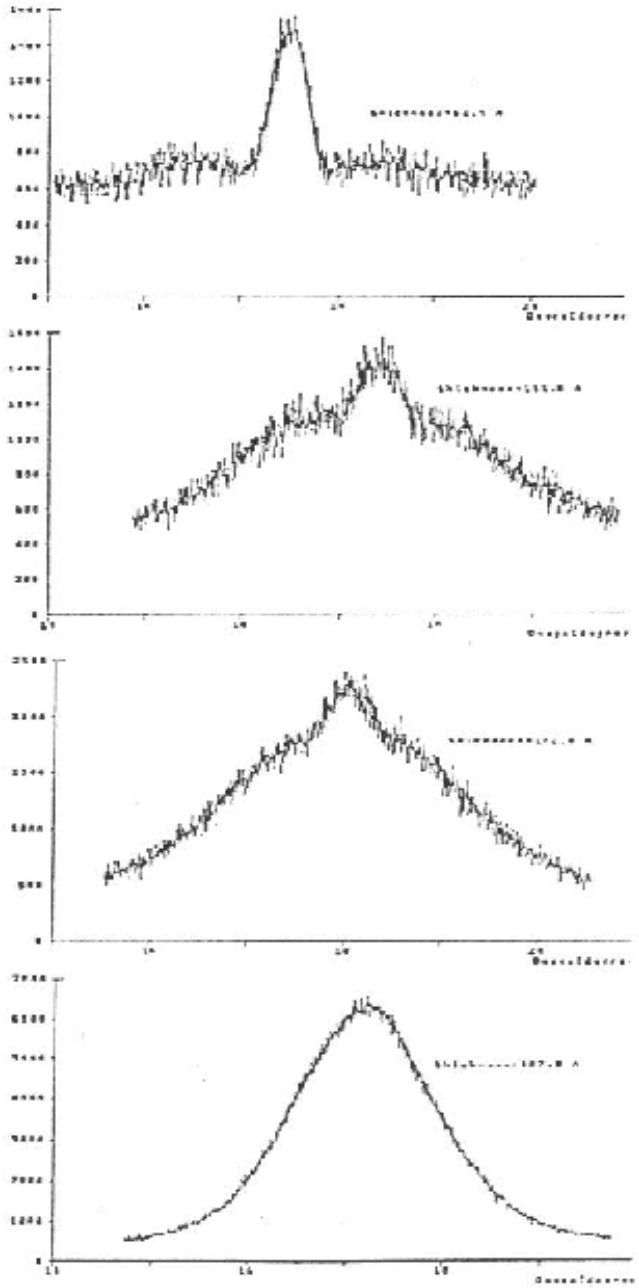

Fig. 12

The ω peaks for thicknesses (from above) [Å]: 52.1, 122.0, 172.0, 487.0

Despite the fact that the order of the chemical reaction was not determined, the linear fits show that the deposition rate is faster at the beginning. Unfortunately, it is not possible to determine boundary conditions where and how the deposition rate slows down to its constant value. As well the plots show that the deposition is not just a physical process. From plots of the single etched , single not etched, and two halves samples one can see different patterns (Fig. 13). The plots of single etched samples do not have so consistent data points as for samples with a native oxide or the halves samples where one half was etched and the other not. The plots of cut-in-half samples (Fig. 14) clearly show that a deposition is not independent of each half. The plots of samples with a native oxide got a different fit value, too. The results of linear fit data of the plots are in the Table 3 and Fig. 15.

The column Poly/Lin is a ratio of the two deposition rates. The samples were sorted into four groups; single grown samples either etched (jk1022dip) or with an oxide (jk1026oxi, jk1027oxi), cut samples either etched (jk1015dip, jk1017dip, jk1018dip, jk1020dip) or with an oxide (jk1015oxi, jk1017, jk1018oxi, jk1020oxi) were considered to compute the activation energy E_a. The suitable deposition were run at 500, 550, 600, 650 °C but only the latter three groups satisfied conditions, two different temperatures, to compute the activation energy. The computing was executed for an average when two or more data were available. The data were substituted to the Arrhenius equation

$$k = A*\exp[E_a/R/T] \quad (28)$$

Because the frequency factor A should be constant for any temperature and it is always considered constant for a certain range of temperature, then the Arrhenius equation can be manipulated to

$E_a = R/(1/T_2 - 1/T_1)*\ln[r_1/r_2]$ (29)

where $r = k*fn[C/_A, C_B, ...]$ is substituted for *k*, and $fn[C_A, C_B, ...]$ cancel each other.

Linear Fit:

single sample with an oxide

$E_a = R/(1/873\ K - 1/773\ K)*\ln[0.363/0.397] \approx 5.0$ kJ/mole

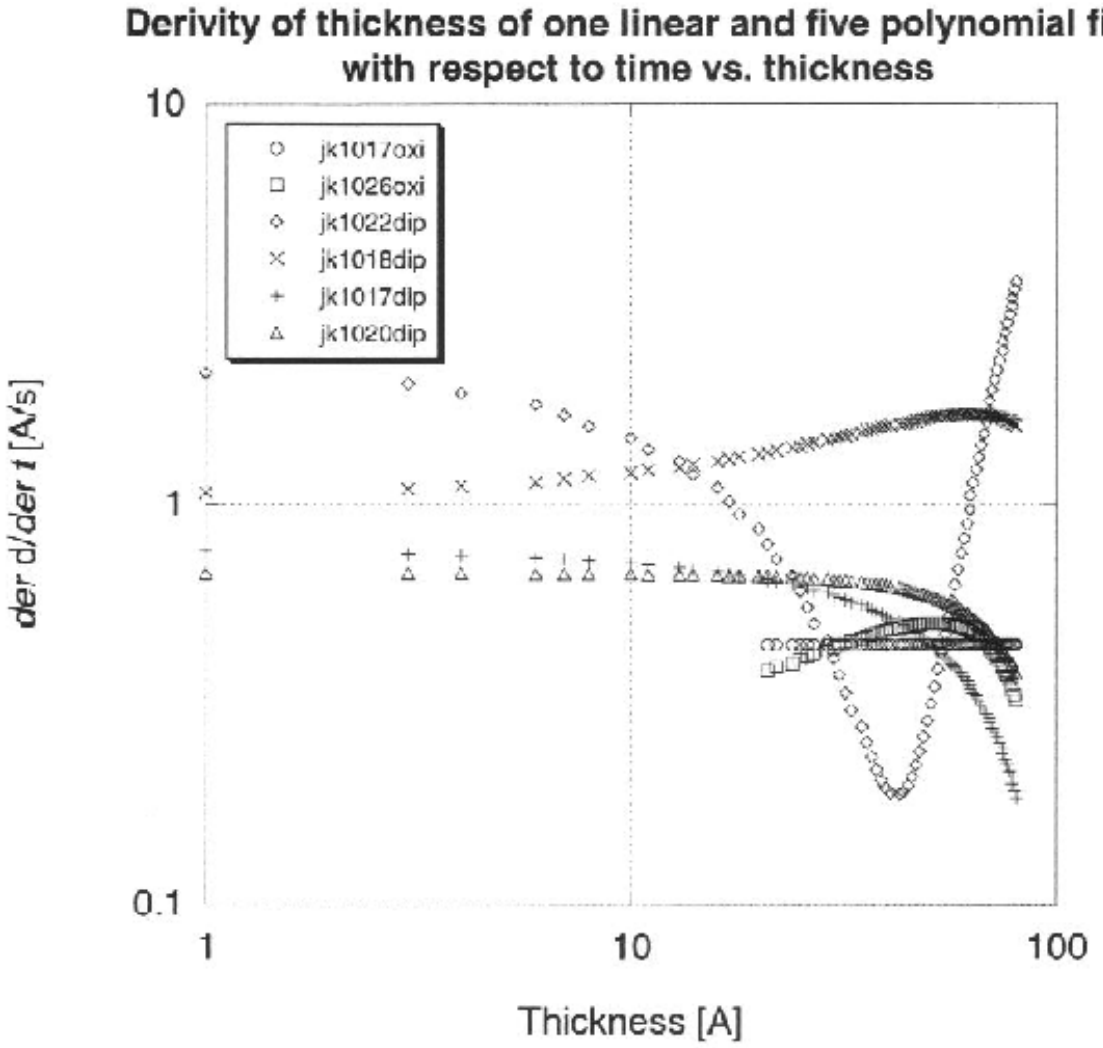

Fig. 13

Plots to determine the order of reaction

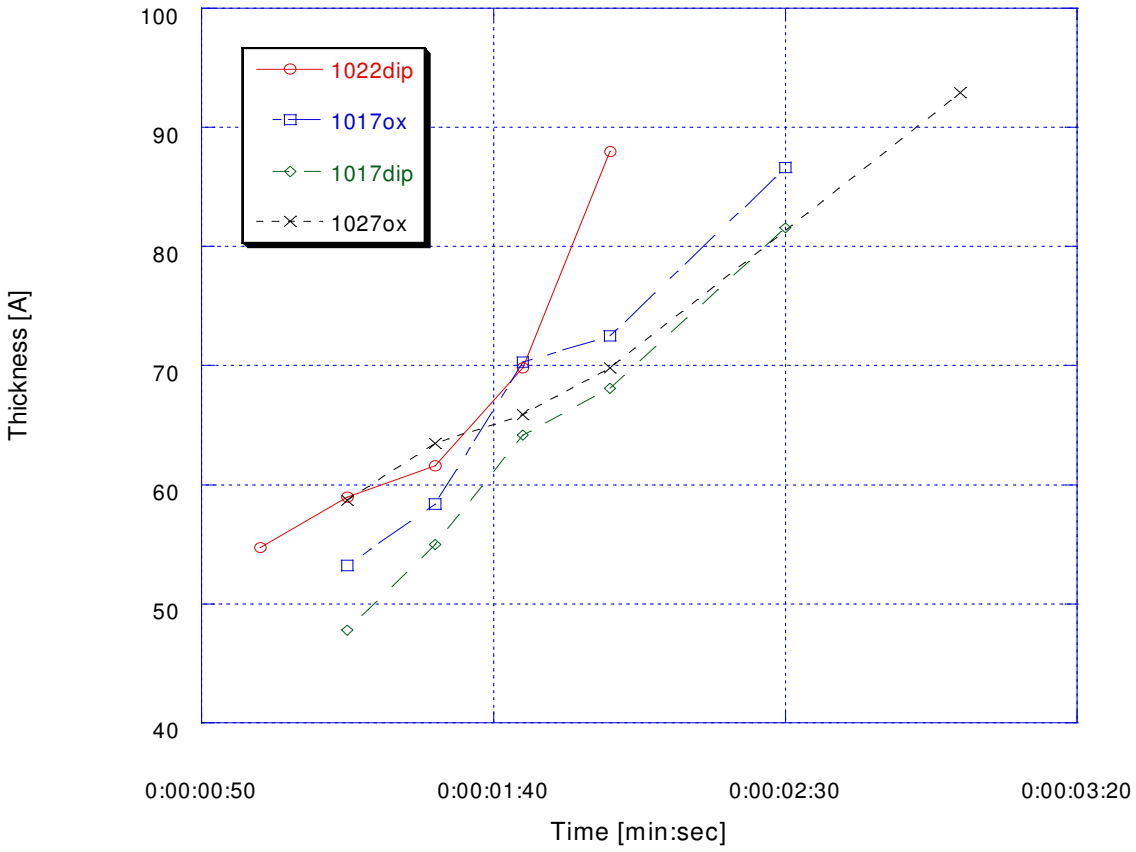

Fig. 14

Four different samples

Etched and unetched singles, etched and unetched halves

sample	thickness [Å] vs. time [s]	sample	thickness [Å] vs. time [s]
jk1015dip	37.981 + 0.280*t	jk1015oxi	21.9 + 0.403*t
jk1017dip	15.197 + 0.446*t	jk1017oxi	19.892 + 0.447*t
jk1018dip	19.309 + 0.402*t	jk1018oxi	20.672 + 0.422*t
jk1020dip	17.232 + 0.451*t	jk1020oxi	31.259 + 0.385*t
jk1022dip	20.18 + 0.516*t	jk1026oxi	26.467 + 0.363*t
jk1027dip	32.962 + 0.328*t		

Table 3

The linear fit data

cut sample with an oxide

E_a = R/(1/923 K - 1/773 K)*ln[(0.503+0.540)/(0.536+0.514)] ≈ 2 kJ/mole

cut sample etched

E_a = R/(1/923 K - 1/773 K)*ln[(0.542+0.649)/(0.662+0.620)] ≈ 2.9 kJ/mole

Polynomial Fit (time = 0):

single sample with an oxide

E_a = R/(1/873 K - 1/773 K)*ln[0.05/0.884] = 161.2 kJ/mole

cut sample with an oxide

E_a = R/(1/923 K - 1/773 K)*ln[1.4+0.655)/(0.793+0.642)] ≈ -14.2 kJ/mole

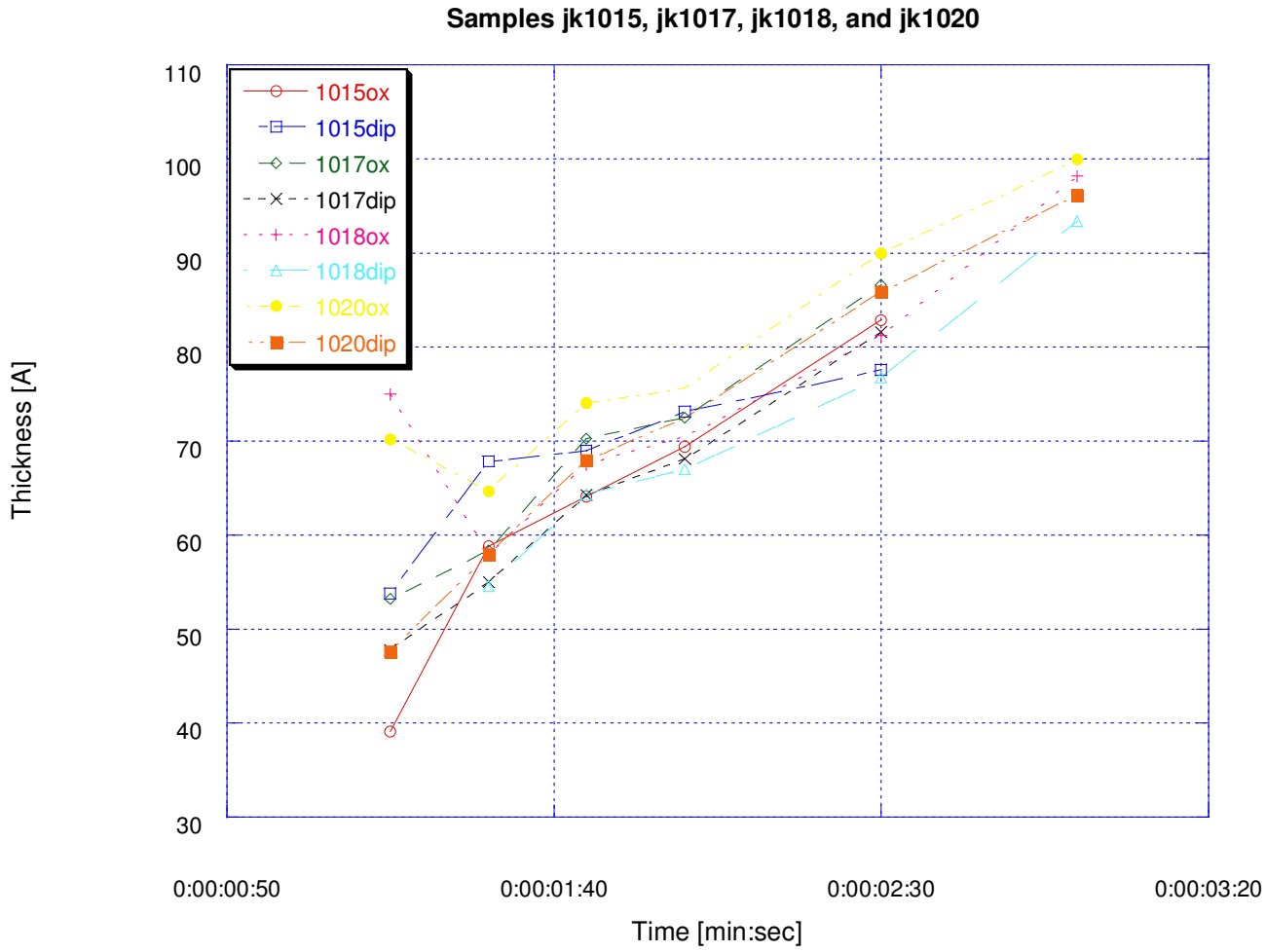

Fig. 15

The plots of the cut samples grown together

cut sample etched

E_a = R/(1/923 K - 1/773 K)*ln[0.779+0.876)/(1.322+1.114)] ≈ 15.3 kJ/mole

As seen from the calculations, the activation energy has relatively a wide range of values. The negative value for the cut sample with an oxide could mean that the reaction in not elementary. All values are under 200 kJ/mole, which means that chemical bonds produced by the plasma sputtering are weak. Some of them are very close to a zero and it could mean that the bonds are created by van der Waals forces. As well as the van der Waalls forces are the main reason why the deposition rate is bigger at the beginning. Another conclusion may emerge from the data, and it is that different compounds take influence on each other despite that the plasma conditions prevail. The plots with the off-points data support this idea because all the points (lower or higher depositions, see Fig. 16 and 17) are for the first runs but one (jk1024). Since some of samples are singles, there is probably an influence between a sample and its surroundings, e.g. walls. Of course, another source of the discrepancy is a human factor. It may have gone by slightly different way when the each equipment was switching on and it may explain a point off in the middle of run but not that most of the off-points are at the beginning.

VIII. EXAMINATION OF THIN FILMS

These films were grown at different temperatures and a Deposition time was always 1 minute. A thickness, theta angle, FWHM of omega, lattice parameter, and lattice mismatch were recorded in the Table 5. All samples were cut in a half. One half was etched in HF and the other not. Both together were put to the chamber and a film was deposited on them at the same time as for some samples that were run to examine a growth rate. The mismatch was usually much less than 1% but each sample got a lattice parameter smaller than 5.403 Å, the lattice parameter of Si. The critical point of view was how the FWHM was changing with temperature. The scans of ω peaks do not sow any significant changes with a temperature (Fig. 18). The FWHM of the peaks are in a range from 0.6° to 1.1°. The higher limit of the FWHM could be questionable because of low intensities of the thin films.

sample	Lin. fit rate	Pol. fit rate	Ratio Pol/Lin	T [K]
	[Å/s]	[Å/s]		
jk1015dip	0.542	0.799	1.474	773
jk1015oxi	0.503	1.4	2.783	773
jk1017dip	0.662	1.322	1.997	923
jk1017oxi	0.536	0.793	1.479	923
jk1018dip	0.62	1.144	1.845	923
jk1018oxi	0.515	0.642	1.247	923
jk1020dip	0.649	0.876	1.35	773
jk1020oxi	0.541	0.655	1.211	773
jk1022dip	0.681	2.256	0.139	823
jk1026oxi	0.363	0.05	0.981	773
jk1027oxi	0.397	0.884	2.227	773

Table 4

The growth rates, their ratios, and temperatures

IX. EXAMINATION OF ELECTRICAL PROPERTIES OF THIN FILMS

The C-V characteristics (Fig. 19 was obtained for example jk0419a) were performed to compute the relative permittivity and current leakage for the YSZ films. The examination was made with films grown at different temperatures and with different resulting thicknesses. Two samples with SiO2 thin films were examined to determine the kind of error that occurred in these experiments. Since the both films (d = 56.3 Å, 124.0 Å) also yield a very low measured relative permittivity (k = 0.24, 0.45) the error is probably in the deposition of Al. Of course, one can not exclude inconsistent deposition of YSZ of the first one or two layers. The inconsistency emerges mainly from the capacitance versus frequency characteristics. The gate capacitance for the lowest frequency is at least three time higher than for the highest frequency. Results of four out of nine samples are given in the Table 5. The samples in the Table 5 showed higher capacitance than the other.

The I-V characteristics were performed along with C-V measurements for three samples from the previous measurements along with six other samples including the two with SiO_2 films (Table 6). The conductance G was recorded for each voltage and Ohm's Law was used to compute the current I. The dot area was 0.525 mm^2 on average. The current density *I* is simply the current I over the dot area with units A/cm^2. The current density limit for the CMOS production is 0.001 $A.cm^2$. Only previous student's sample P227 satisfies this condition. Despite the fact that the FWHM of the sample is 1.35°, which is high. The other YSZ samples under consideration exhibit higher current density, a few hundredths of A/cm^2 at +3.5 V, regardless of thickness. This is satisfactory by some way for the sample jk0928f with the thickness d = 43.9 Å because its thickness is lower than in [9] and the leakage current is lower (Fig. 20 bottom and Fig. 21).

Because the relative permittivity constants were very low, the doping concentration was computed using the Eqn. 11 and compared to the doping concentration obtained from wafer resistivity. The comparisons are in the Table 7 and all of them are fair close except two, which are from samples with very thin films. This mean that the lower capacitance is due to rather improper deposition of aluminum on the films than the film deposition itself.

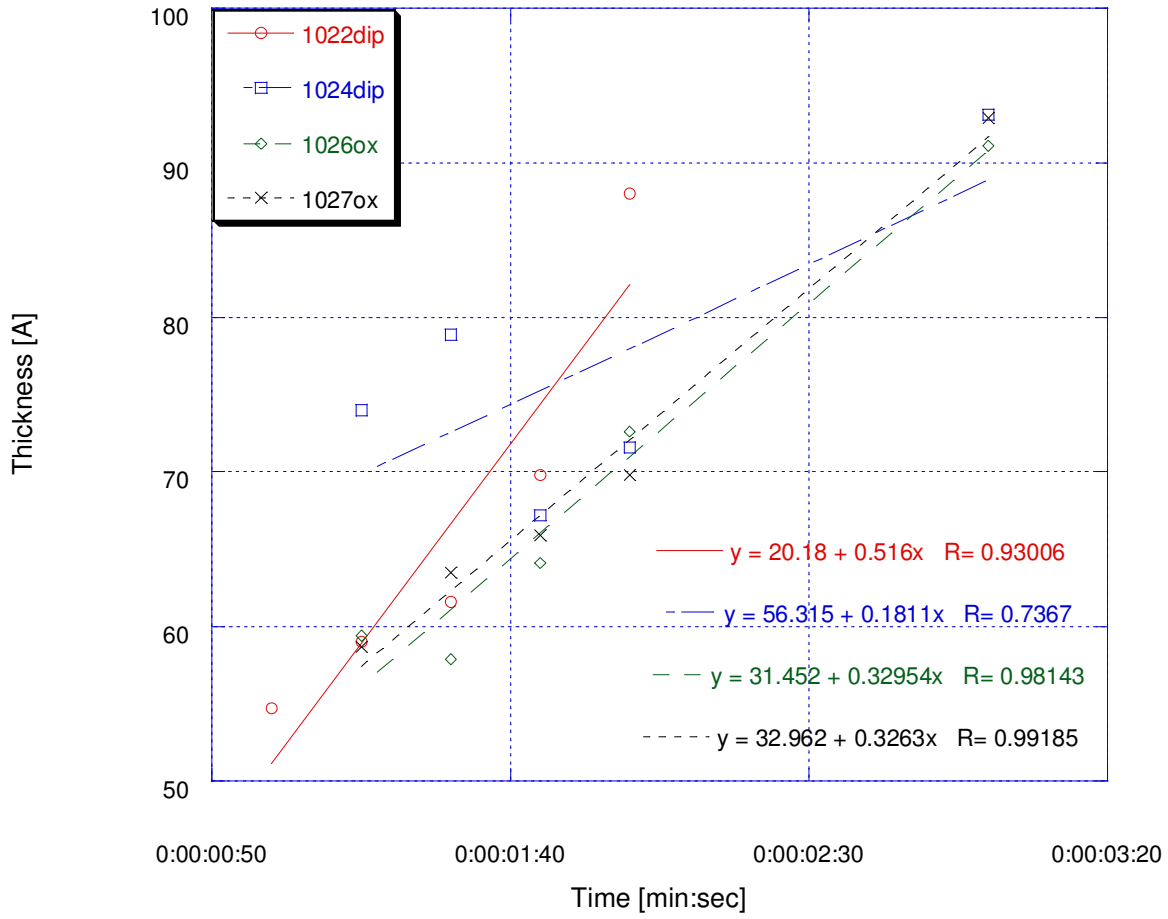

Fig. 16

Discrepancy of jk1024dip and jk1022dip

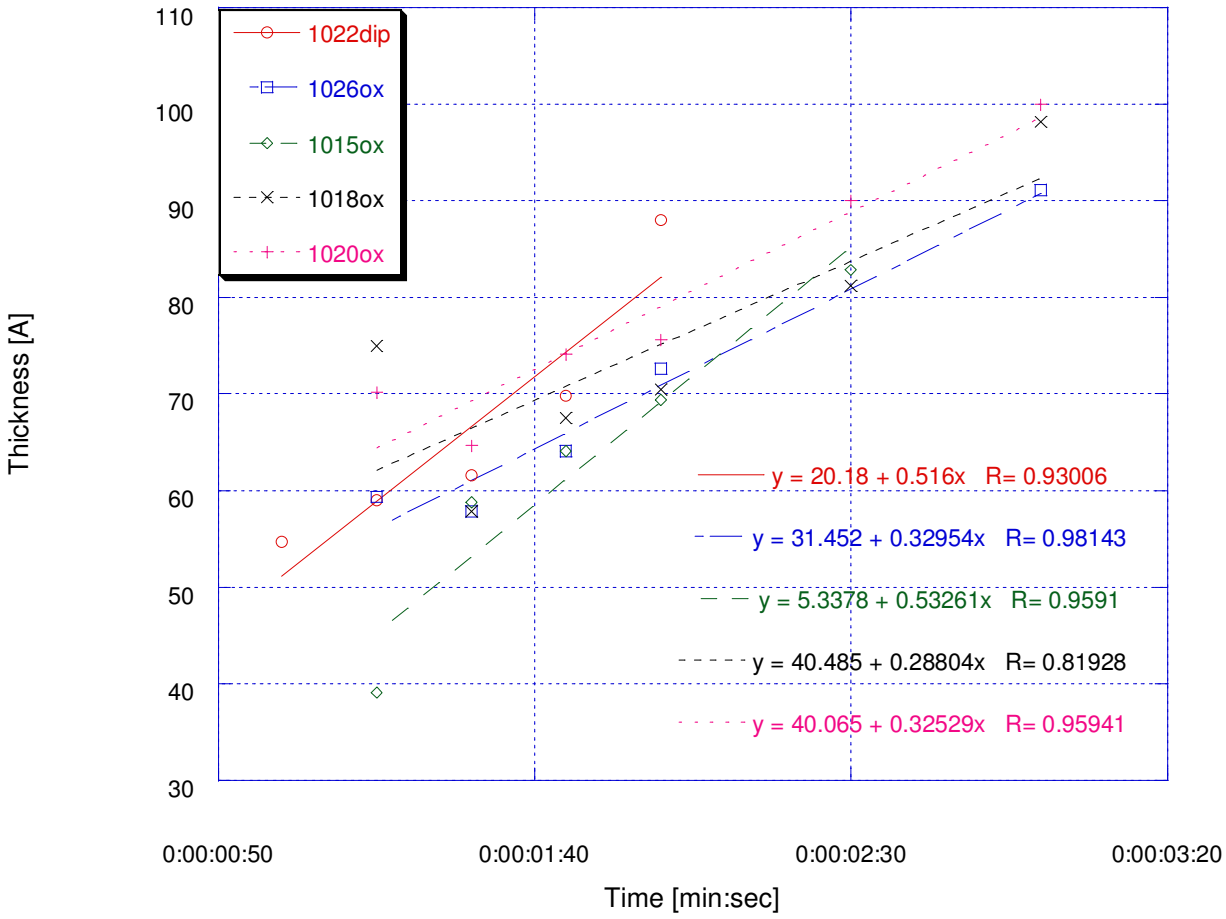

Fig. 17

One point discrepancy of several samples

sample		T [°C]	FWHM [°]	a(YSZ) [Å]	mismatch [%]	thickness [Å]
1001c	not etched	27	0.637	5.418	0.23	NA
1001d	etched	27	0.697	5.366	1.19	NA
1011a	not etched	300	0.708	5.411	0.36	NA
1011a	etched	300	0.813	5.422	0.16	NA
1002f	not etched	400	0.400	5.370	1.12	60.3
1002f	etched	400	0.737	5.422	0.16	NA
1011b	not etched	500	0.660	5.416	0.36	NA
1011b	etched	500	0.842	5.415	0.29	NA
1011c	not etched	600	0.789	5.419	0.22	NA
1011c	etched	600	0.789	5.409	0.40	NA
1011d	not etched	700	0.829	5.418	0.23	NA
1011d	etched	700	0.816	5.417	0.25	NA
1011e	not etched	750	0.803	5.395	0.66	54.1
1011e	etched	750	0.400	5.420	0.20	46.1
1011f	not etched	800	0.866	5.421	0.20	
1011f	etched	800	0.600	5.316	2.18	NA

Table 5

The samples with 1min. deposition grown at different temperatures

frequency [Hz]	C_{1011b}-oxi [pF]	C_{1011b}-dip [pF]	C_{1015b}-oxi [pF]	C_{1015b}-dip [pF]
1E04	345.3	478.0	417.8	268.0
2E04	316.8	441.7	307.9	257.8
4E04	277.7	368.3	217.3	238.4
1E05	213.1	173.5	145.1	203.6
2E05	171.3	62.4	114.9	174.9
4E05	141.3	19.0	95.9	150.5
1E06	112.2	3.8	80.2	125.1
2E06	103.5	1.1	77.6	113.7
4E06	108.4	0.3	85.7	117.8

Table 6

The changes of capacitance with frequency

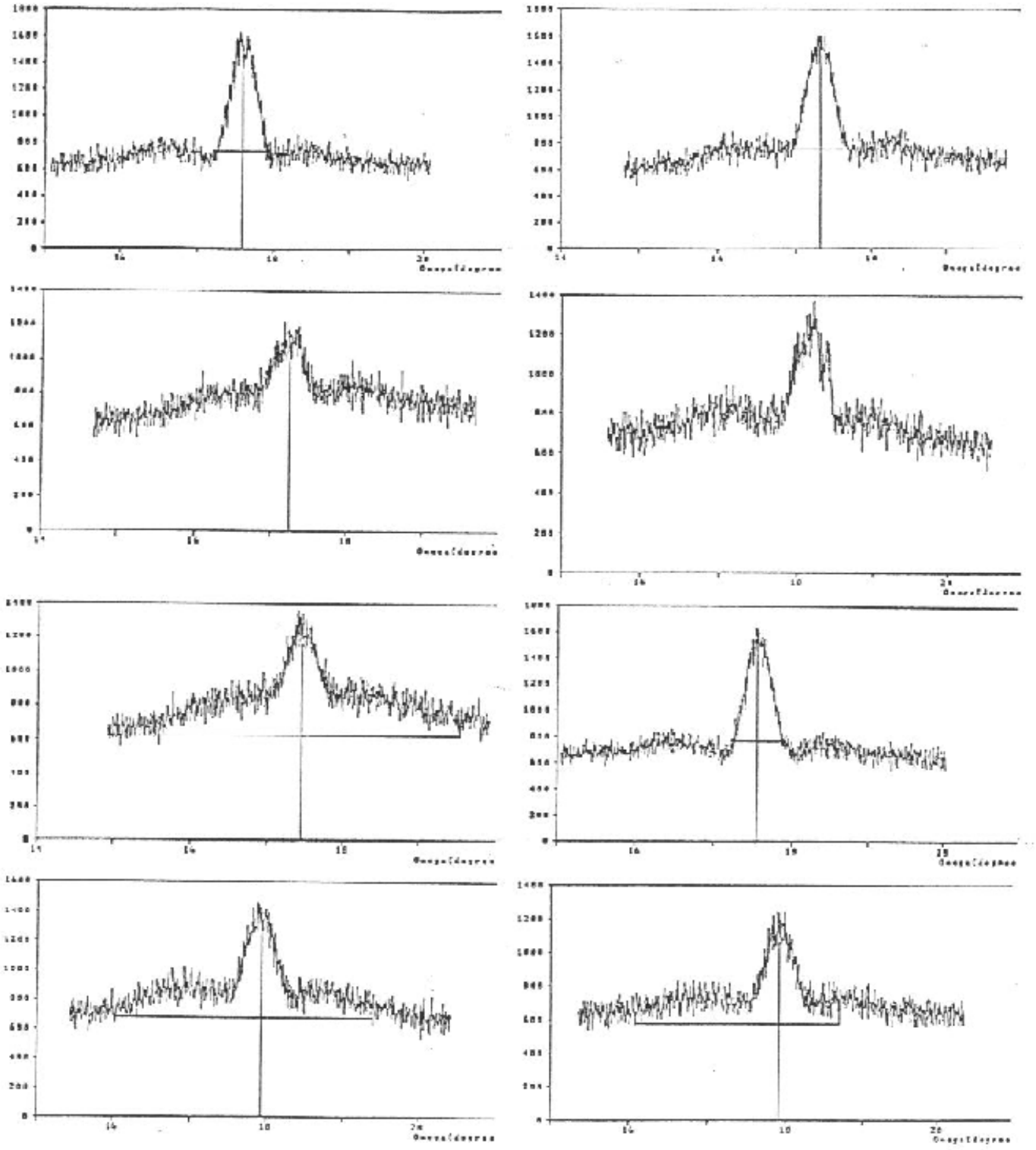

Fig. 18

The ω peaks of samples grown at 27, 400, 600, and 800 °C

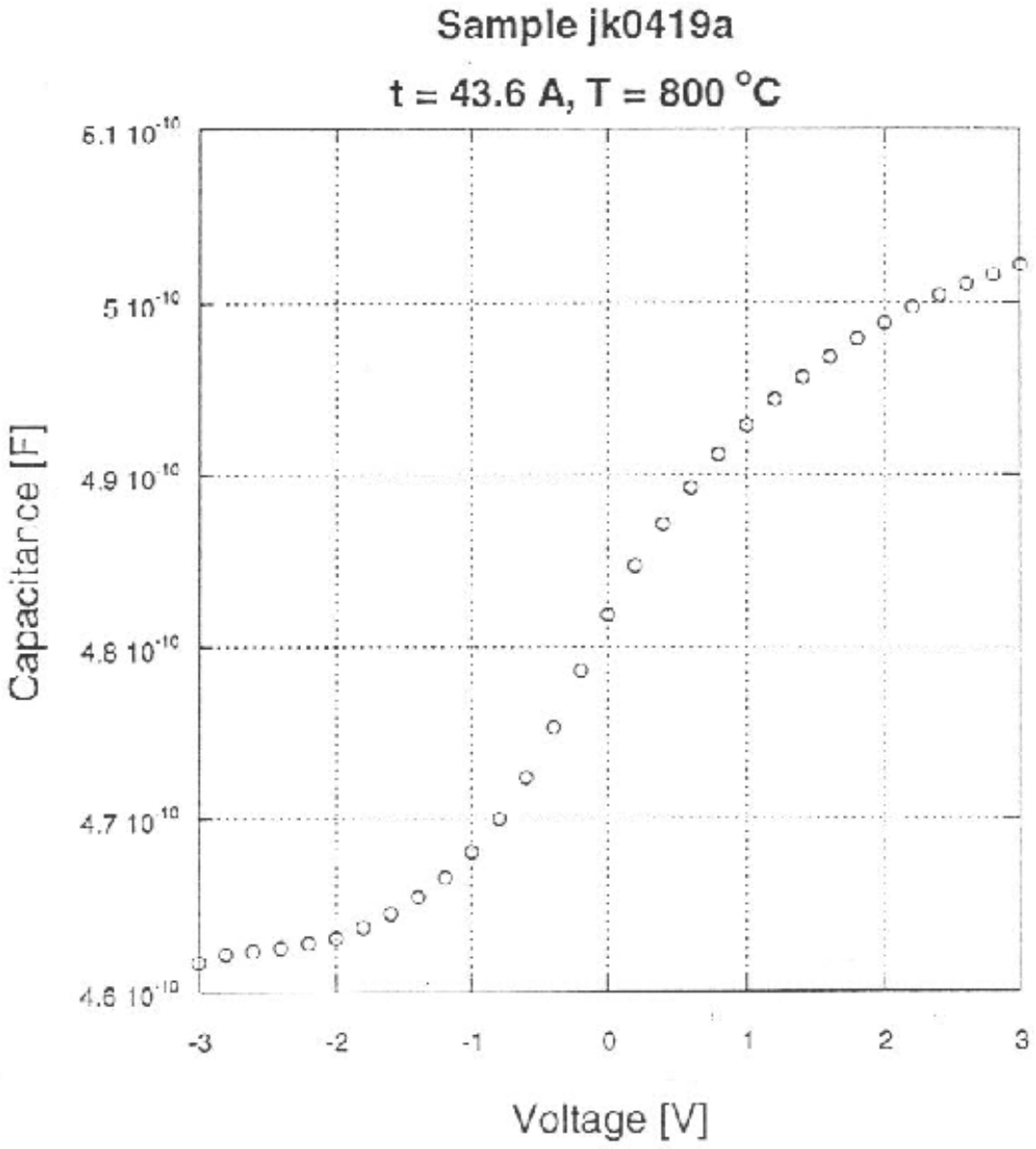

Fig. 19

The C-V characteristics curve of jk0419a

sample	P192c	P227c	jk0419a	jk1011b	jk1015-del	jk1015-phi	jk0928f	jk0111a-SiO_2	jk0111b-SiO_2
T [°C]	800	800	730	500	500	500	800	1050	1050
t [Å]	1025	941	227	35	39.1	53.9	43.9	124	56.3
type	p	n	p	n	n	n	n	p	p
C(ac) [pF]	342.2	329	502.2	91.8	58.2	99.4	65.2	167.8	197.4
C(in) [pF]	90.1	47.6	460.7	28.9	25	60	30	20.2	40.4
FWHM [deg]	0.29	1.35	0.3	0.84	NA	NA	0.76	NA	NA
relative permittivity	7.54	6.66	2.45	0.07	0.05	0.12	0.06	0.45	0.24
N(rho) [cm^{-3}]	1E15	1E15	3E18	1E15	1E15	1E15	1E15	1E15	1E15
N(eqn) [cm^{-3}]	4.93E15	8.26E14	1.68E19	4.83E14	5.25E14	7.82E15	8.83E14	1.57E14	7.26E14
V(FB)	1.5	-0.1	1.5	0.2	-1.8	-0.9	-1.5	-0.3	-0.5

Table 7

The data of samples that were performed for the I-V characteristics

T = temperature of substrate, type = type of substrate,

C(ac) = capacitance from C-frequency plot, C(in) = capacitance from C-V plot,

N(rho) = doping according to resistivity, N(inv) = doping according to Eqn. 11,

V(FB) = flat band voltage

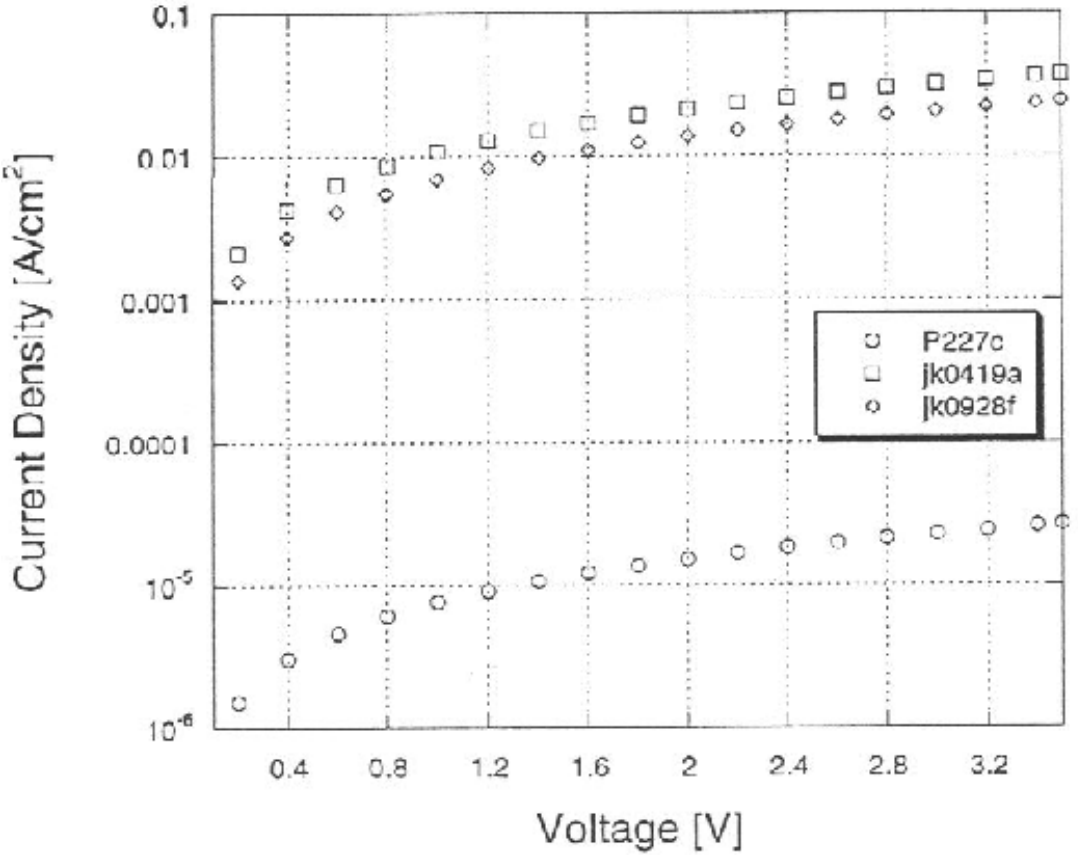

Fig. 20

The I-V characteristics of P227c, jk0419a, and jk0928f

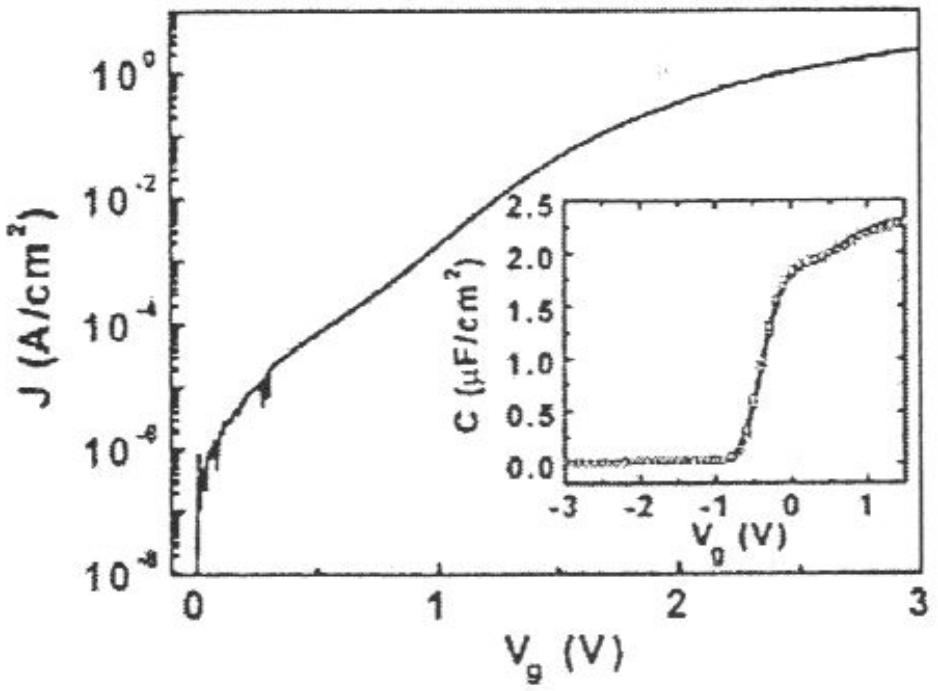

Fig. 21

The I-V characteristics of YSZ with the thickness t = 60 Å deposited by the Electron Beam Epitaxy [2]

X. CONCLUSION

The YSZ exhibits two physical phenomena, which were not described at any article known to the author of this thesis.

The first one is the change of the ω peaks with the increasing film thickness as the result of transition. The YSZ is deposited with significantly more narrow ω peak for approximately the first 100 Å and under certain conditions, the YSZ can be grown to greater thickness with FWHM = 0.3° of the ω peak.

The other phenomenon is that the deposition growth rate is faster at the very beginning. This discovery is crucial to manage the deposition without any inferior layer, which decreases the relative permittivity constant *k* of the YSZ film.

XI. LITERATURE

[1] Wink G. D., Wallace R. M., Anthony J. M.: "High-k gate dielectrics: Current status and materials properties considerations", Applied Physics Review, Vol. 89, MAY 2001, pp. 5243 - 5275

[2] Wang S.J., Tjiu W.C., Yoo W.J.: "Crystalline zirconia oxide on silicon as alternative dielectrics", Applied Physics Letters, Vol. 78, MAR. 2001, pp. 1604-1606.

[3] Wyckoff R.: "Crystal Structures", Interscience Publishers, 2nd Edition, 1963

[4] Hirai T., Teramoto K,. Koike H., Nagashima K., Tarui Y.: "Initial Stage and Growth Process of Ceria, Yttria-Stabilized-Zirconia and Ceria-Zirconia Mixture Thin Films on Si(110) Surfaces",, Jpn. J. Appl. Phys., Vol. 36 (1997), pp. 5253 - 5258

[5] Cullity B., D.: "Elements of X-ray Diffraction", 2nd Edition, Addison-Wesley Publishing Co., 1978

[6] Schroder D. K.: "Semiconductor Material and Device Characterization", 2nd Edition, John Wiley & Sons, Inc., 1998

[7] Fogler H. S.: "Elements of Chemical Reaction Engineering", 2nd Edition, Prentice Hall, 1992

[8] Bardal A., Matthée T., Wecker J., Sawer K.: "Initial stages of Epitaxial Growth of Y-stabilized ZrO_2 Thin Films on a-SiO_x/Si(001) Substrates", J. Appl. Phys. 75 (6), 1994, pp. 2902 - 2910